

VIP **Magnetic Resonance Imaging** Very Important PaperInternational Edition: DOI: 10.1002/anie.201509858  
German Edition: DOI: 10.1002/ange.201509858 **Imaging Glycosylation In Vivo by Metabolic Labeling and Magnetic Resonance Imaging**

André A. Neves,\* Yéléna A. Wainman, Alan Wright, Mikko I. Kettunen, Tiago B. Rodrigues, Sarah McGuire, De-En Hu, Flaviu Bulat, Simonetta Geninatti Crich, Henning Stöckmann, Finian J. Leeper, and Kevin M. Brindle

**Abstract:** Glycosylation is a ubiquitous post-translational modification, present in over 50% of the proteins in the human genome,<sup>[1]</sup> with important roles in cell–cell communication and migration. Interest in glycome profiling has increased with the realization that glycans can be used as biomarkers of many diseases,<sup>[2]</sup> including cancer.<sup>[3]</sup> We report here the first tomographic imaging of glycosylated tissues in live mice by using metabolic labeling and a gadolinium-based bioorthogonal MRI probe. Significant *N*-azidoacetylgalactosamine dependent  $T_1$  contrast was observed in vivo two hours after probe administration. Tumor, kidney, and liver showed significant contrast, and several other tissues, including the pancreas, spleen, heart, and intestines, showed a very high contrast (>10-fold). This approach has the potential to enable the rapid and non-invasive magnetic resonance imaging of glycosylated tissues in vivo in preclinical models of disease.

Various probes have been reported for imaging glycosylation in vivo, including antibodies,<sup>[4]</sup> peptides,<sup>[5]</sup> boronic acid derivatives,<sup>[6]</sup> and lectins.<sup>[7]</sup> Most approaches give a static view of cell-surface glycosylation. We, and others, have used metabolic glycan labeling<sup>[8]</sup> in combination with bioorthogonal reactions<sup>[9]</sup> to image the dynamics of glycan biosynthesis in vivo. We demonstrated non-invasive imaging of tumor glycosylation in live mice<sup>[10]</sup> by metabolic labeling of tumor

glycans with azido sugars followed by Staudinger ligation with a biotinylated phosphine and subsequent imaging using fluorescent or radionuclide-labeled avidins. More recently, we described “double-click” reagents,<sup>[11]</sup> where azido-modified cell-surface glycoproteins were detected using a bivalent double-click bioorthogonal probe. The latter consisted of a strained tetramethoxydibenzocyclooctyne (TMDIBO),<sup>[12]</sup> which reacted specifically with azido sugar labeled glycans,<sup>[9]</sup> and a *trans*-cyclooctene (TCO), which reacted very rapidly with a fluorescently labeled tetrazine for fluorescence imaging (FLI). FLI gives high sensitivity and throughput,<sup>[13]</sup> however, a limitation is light absorption and scattering, which prevents deep imaging in opaque organisms such as mice.

Recently, cells metabolically labeled with *N*-azidoacetylmannosamine were imaged by magnetic resonance imaging (MRI) and a xenon (<sup>129</sup>Xe) biosensor. The azido group in cell-surface sialic acid residues was detected using a bifunctional reagent incorporating bicyclo[6.1.0]nonyne, which reacted with the azido group, and a cryptophane, which bound hyperpolarized <sup>129</sup>Xe. Bound xenon was detected by magnetization transfer measurements between free and bound xenon (hyper-CEST).<sup>[14]</sup> Although hyperpolarized <sup>129</sup>Xe is very sensitive to MR detection, the change in signal intensity was relatively small (ca. 30–50%), and only demonstrated for encapsulated cells in a bioreactor. A CEST-based label-free method for imaging underglycosylated mucin-1 expression in vivo has also been described recently.<sup>[15]</sup>

Our aim was to develop a probe for the tomographic, non-invasive MR imaging of metabolically labeled glycans in mice. A previously reported MRI probe, consisting of a phosphine conjugated to a gadolinium chelate,<sup>[11]</sup> gave no detectable azido sugar dependent contrast in vivo owing to high levels of non-specific binding, which we attributed to its hydrophobicity. We describe here TMDIBO–Lys–Gd (**2**; Figure 1), a novel water-soluble probe that combines a strained cyclooctyne TMDIBO linked, via a hydrophilic lysine linker, to a gadolinium DOTA chelate, a clinically approved MRI contrast agent.<sup>[16]</sup> This probe was used to image metabolically labeled cell-surface glycans on tumor cells in vitro and in vivo. The probe also showed significant labeling of other mouse tissues, including the pancreas, spleen, kidney, liver, and gut.


The  $T_1$  relaxivity of **2** (Figure 1) in buffer at 7 T was  $6.3 \pm 0.1 \text{ mM}^{-1}\text{s}^{-1}$ , similar to published values for Gd DOTA complexes.<sup>[16]</sup> The reactivity of **2** with cell-surface azido sugar labeled glycans was determined by culturing Lewis lung (LL2) adenocarcinoma cells with *N*-azidoacetylgalactosamine (Ac<sub>4</sub>GalNAz, **1**; Figure 1) for 24 h, and then incubating


[\*] Dr. A. A. Neves, Dr. Y. A. Wainman, Dr. A. Wright, Dr. M. I. Kettunen,<sup>[†]</sup> Dr. T. B. Rodrigues, S. McGuire, Dr. D.-E. Hu, Prof. K. M. Brindle  
Cancer Research UK Cambridge Institute, Li Ka Shing Centre  
Cambridge CB2 0RE (UK)  
E-mail: andre.neves@cruk.cam.ac.uk

Dr. Y. A. Wainman, F. Bulat, Dr. H. Stöckmann, Dr. F. J. Leeper  
Department of Chemistry, University of Cambridge  
Cambridge CB2 1EW (UK)

Dr. S. Geninatti Crich  
Department of Molecular Biotechnology and Health Science  
Molecular Imaging Center  
Via Nizza 52, 10126 Turin (Italy)

[†] Current address: A. I. Virtanen Institute for Molecular Sciences  
University of Eastern Finland  
Neulaniementie 2, 70211 Kuopio (Finland)

 Supporting information and ORCID(s) from the author(s) for this article are available on the WWW under <http://dx.doi.org/10.1002/anie.201509858>.

 © 2015 The Authors. Published by Wiley-VCH Verlag GmbH & Co. KGaA. This is an open access article under the terms of the Creative Commons Attribution License, which permits use, distribution and reproduction in any medium, provided the original work is properly cited.

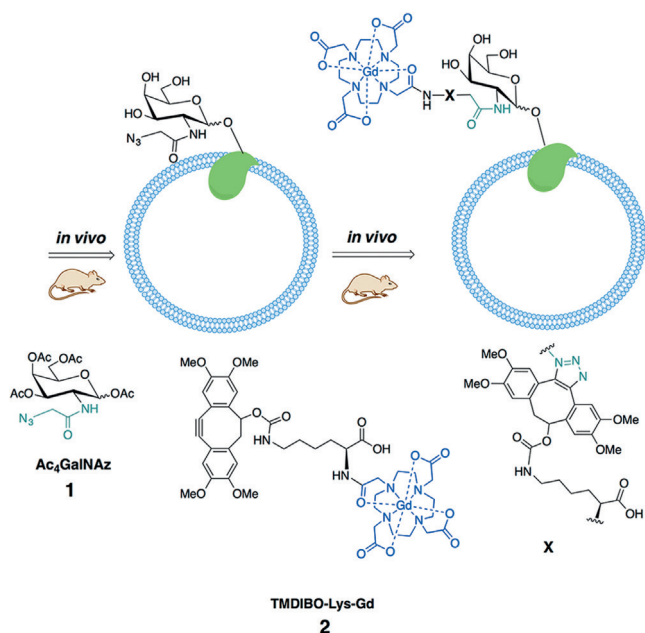


**Figure 1.** Labeling of cell-surface glycans with an MRI-detectable probe. Mice were injected daily with peracetylated *N*-azidoacetyl-galactosamine (Ac<sub>4</sub>GalNAz, **1**). Azido-labeled cell-surface glycoproteins were then detected in vivo by subsequent reaction with a bioorthogonal MRI contrast agent, TMDIBO-Lys-Gd (**2**).

them with **2** for 45 min, after which the cells were washed. The  $R_1$  ( $1/T_1$ ) relaxation rates were measured in pelleted cells that had been incubated with (+/+/-) or without (+/-/-) **1** and/or **2** (+/+ / +, +/- / +; Figure 2). There was a significant increase ( $P < 0.005$ ) in  $R_1$  in azido sugar (**1**) treated LL2 cells that had been incubated with **2** (+/+ / +,  $1.38 \pm 0.10 \text{ s}^{-1}$ ), when compared with cells not cultured with the azido sugar (+/- / +,  $0.79 \pm 0.02 \text{ s}^{-1}$ ) or with cells not incubated with either **1** or **2** (+/- / -,  $0.64 \pm 0.03 \text{ s}^{-1}$ ,  $P < 0.001$ ). The small increase in  $R_1$  (by a factor of  $1.23 \pm 0.01$ ) between cells that

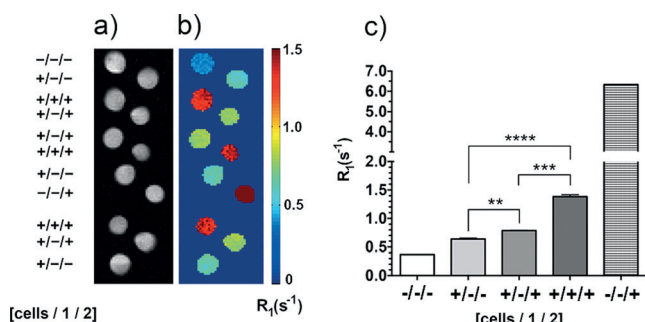


**Figure 2.** MR imaging of cell-surface glycosylation in vitro. a) T<sub>2</sub>-weighted images and b) corresponding maps of the  $R_1$  relaxation rates ( $1/T_1$ ). The images were obtained from cell pellets of untreated cells (+/-/-), cells treated with solvent vehicle and **2** (1.0 mM, for 45 min at 37°C; +/- / +), or cells incubated with **1** (50 μM, for 24 h at 37°C) and **2** (1.0 mM, for 45 min at 37°C; +/+ / +). The  $R_1$  rates were also measured in the buffer in which the cells had been suspended (-/- / -) and in a buffer to which **2** had been added (1.0 mM; -/- / +). Data represent the mean ± standard error of the mean (SEM) ( $n = 3$ ).  $**P < 0.01$ ,  $***P < 0.005$ ,  $****P < 0.001$ . Two-tailed unpaired T-test with Mann-Whitney correction.

had not been treated with either **1** or **2** (+/-/-) and cells incubated with **2** alone (+/- / +) showed that there were only low levels of non-specific binding of **2**. This was considerably less than observed previously with a fluorescently labeled version of TMDIBO, where this ratio was  $3.3 \pm 0.1$ .<sup>[11]</sup>

Mice with flank tumors, obtained by subcutaneous injection of LL2 cells, were injected daily, for three days, with Ac<sub>4</sub>GalNAz (**1**; 300 mg kg<sup>-1</sup>, i.p.) or with solvent vehicle, and then injected with **2** (0.25 mmol kg<sup>-1</sup>, i.v.; gadolinium-based contrast media are used clinically at 0.1–0.3 mmol kg<sup>-1</sup>) on day 4.<sup>[17]</sup> The metabolic labeling of glycans with **1** and subsequent bioorthogonal detection with **2** was confirmed by ICP-MS measurements of the gadolinium content in excised tissues (Figure 3) obtained after the imaging experiments

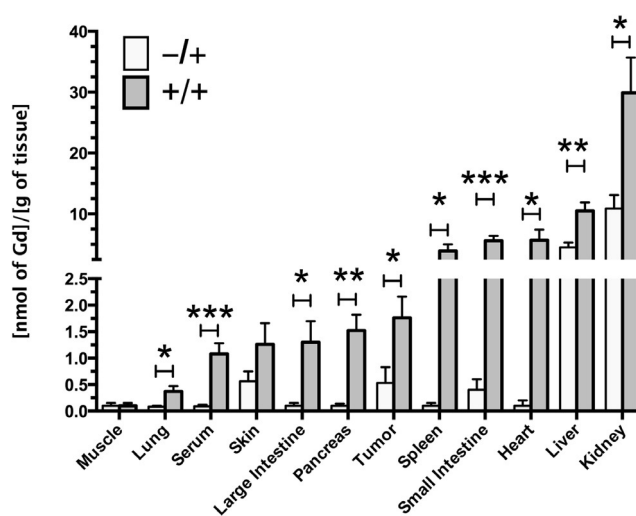


**Figure 3.** Gadolinium concentrations in metabolically labeled mouse tissues. The Gd content of excised tissues was determined by inductively coupled plasma mass spectrometry (ICP-MS). Tissues were obtained from control mice (-/+) and Ac<sub>4</sub>GalNAz treated mice (+/+) after the imaging experiments and 24 h after injection of **2** (Figure 1). The Gd content was normalized to the wet tissue weight. Data represent the mean ± SEM ( $n = 5$ ).  $*P < 0.05$ ,  $**P < 0.01$ ,  $***P < 0.005$ . Two-tailed unpaired T-test with Mann-Whitney correction.

(Figures 4 and 5), and 24 h after the injection of **2**. Most tissues showed *N*-Ac<sub>4</sub>GalNAz dependent labeling. The gadolinium content was highest in the kidney ( $29.9 \pm 5.8$  nmol Gd per gram of tissue). However, about one third of this was due to the non-specific retention of **2** and thus not *N*-Ac<sub>4</sub>GalNAz dependent ( $10.9 \pm 2.2$  nmol Gd per gram of tissue), and metabolic labeling was relatively modest (2.7 ± 0.5-fold increase in gadolinium content in animals injected with **1** and **2** (+/+) compared with those injected with **2** alone (-/+). The high background signal in the kidney is likely due to this organ being the preferred clearance route for molecules < 1 kDa. The liver also showed relatively high levels of non-specific retention of **2** ( $4.5 \pm 0.8$  nmol Gd per gram of tissue) and similar levels of *N*-Ac<sub>4</sub>GalNAz dependent labeling as the kidney ( $2.3 \pm 0.3$ -fold). The levels of kidney and liver labeling are in agreement with our previous work on FLI.<sup>[11]</sup> Other tissues showed very low levels of non-specific

background retention of **2** and consequently high levels of  $N$ -Ac<sub>4</sub>GalNAz dependent labeling. The gadolinium concentration ratios for tissues from animals injected with  $N$ -Ac<sub>4</sub>GalNAz (+/+ ) relative to those injected with the solvent vehicle (-/+ ) were  $57 \pm 8$  for the heart,  $39 \pm 4$  for spleen,  $14 \pm 2$  for the pancreas and the small and large intestine, and  $5 \pm 1$  for the lungs. Tumors showed much higher levels of non-specific retention of **2**, and therefore, the gadolinium concentration ratio was much lower ( $3.3 \pm 1.1$ ). Glycan-labeling methods based on the delivery of labeled sugars using targeted liposomes<sup>[18]</sup> could be used to improve tumor selectivity.

Serum showed significant metabolic labeling (the serum gadolinium concentration ratio for animals injected with  $N$ -Ac<sub>4</sub>GalNAz and those injected with the solvent vehicle was  $12 \pm 1$ ,  $P < 0.005$ ; Figure 3). Metabolic labeling of mouse serum<sup>[19]</sup> is thought to result from the incorporation of azido sugars into the major glycosylated proteins present.<sup>[20]</sup> We

estimated the contribution of labeled serum glycoproteins to labeling of the small intestine, spleen, kidney, and liver from the serum contents of these tissues, which have been estimated to be 5.0, 9.2, 19.1, and 20.2% of the tissue volume, respectively.<sup>[21]</sup> The contribution of labeled serum proteins was estimated to be only 1.0, 2.4, 1.0, and 3.4% of the total tissue glycan labeling, respectively. Tumors have a much larger interstitial volume fraction (20–40%),<sup>[22]</sup> and their leaky neovasculature results in the retention of macromolecules.<sup>[23]</sup> However, the contribution to tumor labeling, due to retention of labeled serum proteins, was estimated to be only 15–30% of the total.

$T_2$ -weighted images and  $T_1$  relaxation rate ( $R_1$ ) maps (Figure 4) were acquired in vivo before and at 2 and 24 h post injection of **2**. The relaxation rates ( $R_1$ ) for water protons in the tumor, kidney, and liver (Figure 4) were significantly higher in animals injected with **1** and **2** (+/+ ) than for the controls injected with the vehicle and **2** (-/+ ), demonstrating

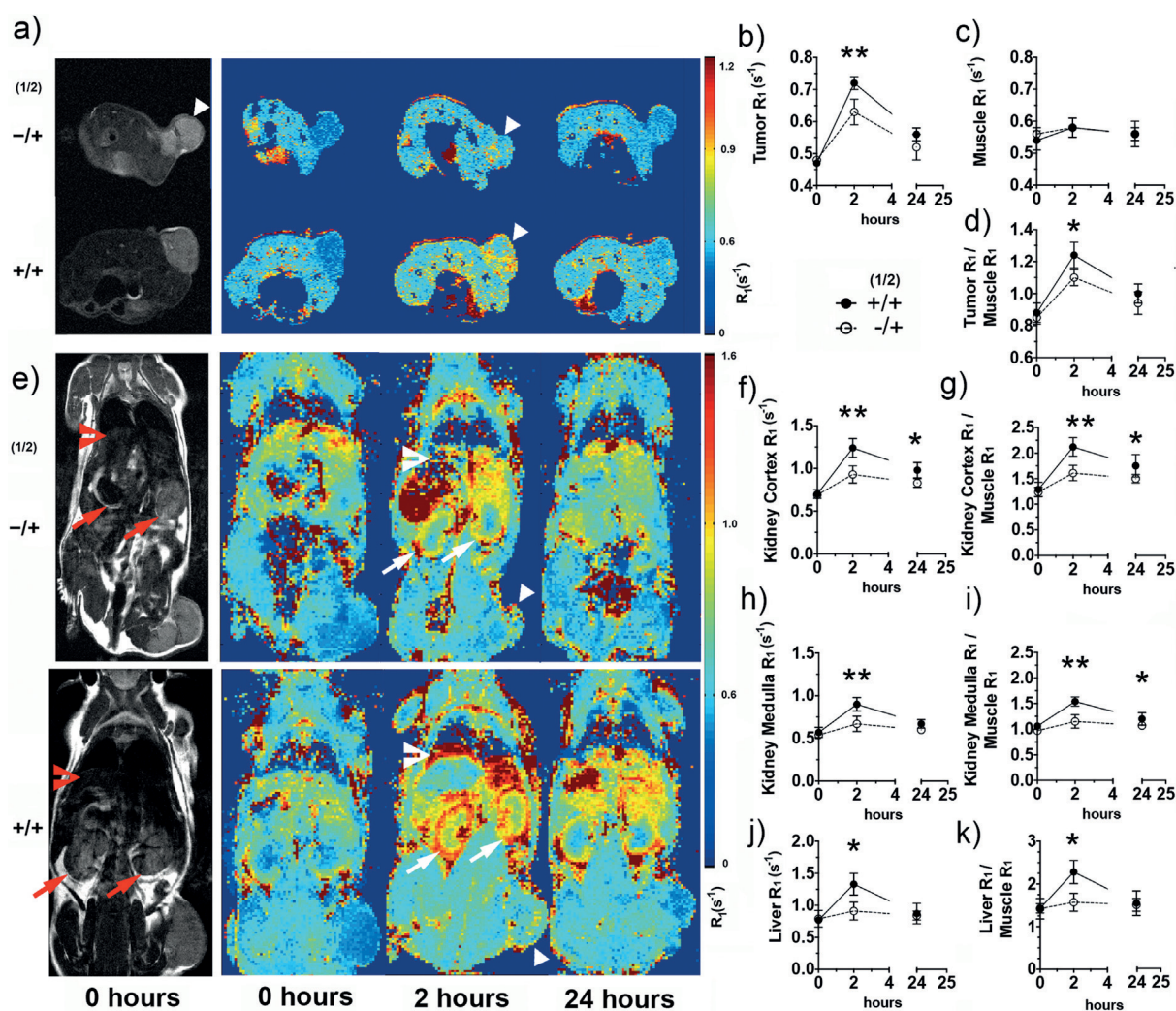


**Figure 4.** Imaging tissue glycosylation in vivo using MRI  $T_1$  maps.  $T_2$ -weighted (gray scale) images (a, e) and  $T_1$  maps (pseudo-colored; a, e) of representative mice injected with the vehicle and **2** (-/+ ) or **1** and **2** (+/+ ), showing metabolic labeling of tumor (triangles), kidney (arrows), and liver (chevrons), 2 and 24 h after injection of **2**. a) Axial and e) coronal images are shown. The kinetics of  $N$ -Ac<sub>4</sub>GalNAz dependent contrast formation were analyzed for regions of interest defined on the  $T_2$ -weighted images for the tumor (b), muscle (c), kidney cortex (f), medulla (h), and liver (j), and the corresponding data were normalized to the muscle data (d, g, i, k). Data in (b)–(d) and (f)–(k) represent mean  $\pm$  SEM ( $n=5$ ). The relaxation rate  $R_1$  ( $1/T_1$ ) is expressed in  $s^{-1}$ . \* $P < 0.05$ , \*\* $P < 0.01$ . Two-tailed unpaired T-test with Mann–Whitney correction.

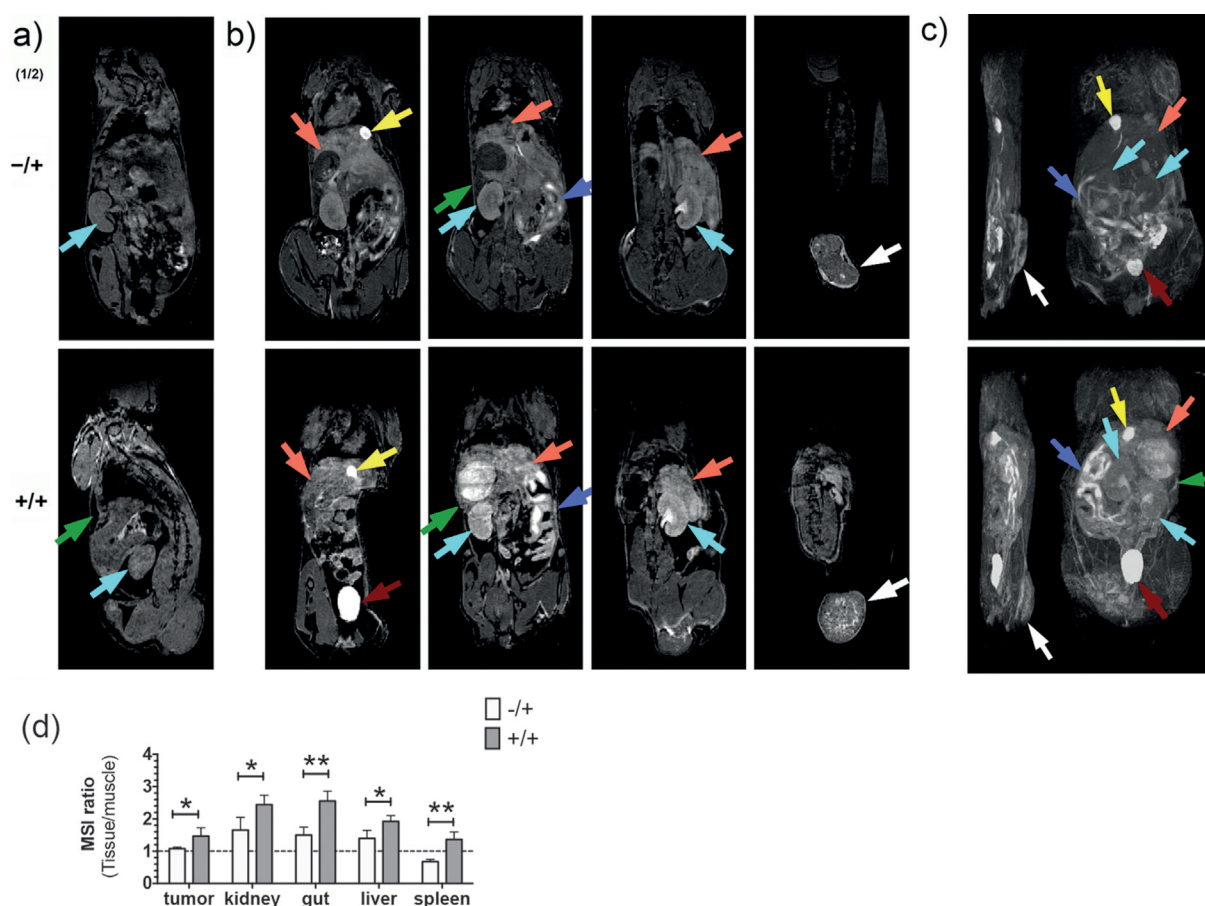


**Figure 5.** Imaging tissue glycosylation in vivo using  $T_1$ -weighted MRI. Coronal  $T_1$ -weighted images, before (a) and 2 h after (b) the injection of **2**. Maximum intensity projection of  $T_1$ -weighted signals (c) from representative mice injected with solvent vehicle and **2** (-/+ ) or **1** and **2** (+/+). Coronal  $T_1$ -weighted images (b, left to right) are displayed from the ventral towards the dorsal side. Maximum intensity projections (c) onto the sagittal (left) and coronal (right) planes. b) Metabolic labeling was observed in the tumor (white arrows), kidney (cyan), liver (orange), gut (purple), and spleen (green) 2 h after the injection of **2**. Bladder and gallbladder are indicated by red and yellow arrows, respectively. d) The  $N$ -Ac<sub>4</sub>GalNAz dependent contrast was analyzed semi-quantitatively, using regions of interest defined in the  $T_1$ -weighted images for the tumor, kidney, gut, liver, and spleen; the mean signal intensity (MSI) for these tissues was divided by the MSI of muscle. Data represent mean  $\pm$  SEM ( $n=4$ ). \* $P<0.05$ , \*\* $P<0.005$ . Two-tailed unpaired T-test with Mann–Whitney correction.

non-invasive MRI detection of  $N$ -Ac<sub>4</sub>GalNAz dependent tissue labeling in vivo (Figure 4b–k).

The tumor contrast observed 2 h after probe injection was similar to that reported recently at 24 h after administration of a boronic acid based MRI contrast agent for detecting sialic acid in a murine model of melanoma.<sup>[6]</sup> Other organs also showed appreciable labeling (Figure 4e, +/+); however, analysis of the  $T_1$  maps was difficult owing to organ motion. A semi-quantitative estimate of labeling based on coronal  $T_1$ -weighted images acquired in vivo (Figure 5 and Movie S1) 2 h post administration of **2** indicated significant azido sugar dependent labeling of tumor ( $P<0.05$ ), kidney ( $P<0.05$ ), gut ( $P<0.005$ ), liver ( $P<0.05$ ), and spleen ( $P<0.005$ ).

The gadolinium concentrations in tumor, kidney, and liver were estimated using the  $T_1$  relaxivity of **2**, and the relaxation rates of these tissues measured in vivo (Figure 4). This gave gadolinium concentrations of  $42 \pm 3$ ,  $80 \pm 6$  and  $93 \pm 12 \mu\text{M}$ , respectively, at 2 h post administration of **2** and  $15 \pm 1$ ,  $38 \pm 3$ , and  $17 \pm 1 \mu\text{M}$  at 24 h. The gadolinium concentration in the kidney measured ex vivo after 24 h was  $30 \pm 6 \mu\text{M}$  (Figure 3),

which is comparable with that estimated by the in vivo experiment. There was poorer agreement between the estimated in vivo concentrations in the tumor and liver at 24 h and those measured ex vivo, which were  $1.8 \pm 0.4$  and  $11 \pm 1 \mu\text{M}$ , respectively (Figure 3). However, this can be explained by the fact that the estimated minimum MRI-detectable tissue concentration of gadolinium is approximately  $10 \mu\text{M}$ .<sup>[24]</sup>

In summary, the gadolinium-labeled bioorthogonal probe described here can be used for the non-invasive in vivo imaging of tissue glycosylation by magnetic resonance imaging. Most tissues showed only low levels of non-specific retention of TMDIBO–Lys–Gd (**2**), and a significant  $N$ -azidoacetyl galactosamine dependent contrast was observed within two hours of probe administration. As altered cell-surface glycosylation is a hallmark of disease, particularly cancer, and MRI is a widely used imaging technique, this novel method may enable the rapid assessment of disease-related changes in glycosylation in vivo.

## Acknowledgements

The work was supported by a Cancer Research UK Programme grant (17242) to K.M.B. and the CRUK-EPSRC Imaging Centre in Cambridge and Manchester (16465). Y.A.W. and F.B. were in receipt of Cancer Research UK Ph.D. studentships.

**Keywords:** bioorthogonal chemistry · cancer · gadolinium · glycans · magnetic resonance imaging

**How to cite:** *Angew. Chem. Int. Ed.* **2016**, *55*, 1286–1290  
*Angew. Chem.* **2016**, *128*, 1308–1312

- [1] M. N. Christiansen, J. Chik, L. Lee, M. Anugraham, J. L. Abrahams, N. H. Packer, *Proteomics* **2014**, *14*, 525–546.
- [2] C. B. Lebrilla, H. J. An, *Mol. Biosyst.* **2009**, *5*, 17–20.
- [3] a) H. J. An, S. R. Kronewitter, M. L. de Leoz, C. B. Lebrilla, *Curr. Opin. Chem. Biol.* **2009**, *13*, 601; b) D. W. Kufe, *Nat. Rev. Cancer* **2009**, *9*, 874.
- [4] S. T. Laughlin, C. R. Bertozzi, *Proc. Natl. Acad. Sci. USA* **2009**, *106*, 12–17.
- [5] P. L. Hsiung et al., *Nat. Med.* **2008**, *14*, 454–458.
- [6] S. Geninatti Crich, D. Alberti, I. Szabo, S. Aime, K. Djanashvili, *Angew. Chem. Int. Ed.* **2013**, *52*, 1161–1164; *Angew. Chem.* **2013**, *125*, 1199–1202.
- [7] E. L. Bird-Lieberman, A. A. Neves, P. Lao-Sirieix, M. O'Donovan, M. Novelli, L. B. Lovat, W. S. Eng, L. K. Mahal, K. M. Brindle, R. C. Fitzgerald, *Nat. Med.* **2012**, *18*, 315–321.
- [8] J. A. Prescher, D. H. Dube, C. R. Bertozzi, *Nature* **2004**, *430*, 873–877.
- [9] C. P. Ramil, Q. Lin, *Chem. Commun.* **2013**, *49*, 11007–11022.
- [10] a) A. A. Neves, H. Stöckmann, R. R. Harmston, H. J. Pryor, I. S. Alam, H. Ireland-Zecchini, D. Y. Lewis, S. K. Lyons, F. J. Leeper, K. M. Brindle, *FASEB J.* **2011**, *25*, 2528; b) R. Rossin, M. S. Robillard, *Curr. Opin. Chem. Biol.* **2014**, *21*, 161.
- [11] A. A. Neves, H. Stöckmann, Y. A. Wainman, J. C. Kuo, S. Fawcett, F. J. Leeper, K. M. Brindle, *Bioconjugate Chem.* **2013**, *24*, 934–941.
- [12] H. Stöckmann, A. A. Neves, S. Stairs, H. Ireland-Zecchini, K. M. Brindle, F. J. Leeper, *Chem. Sci.* **2011**, *2*, 932–936.
- [13] S. Kumar, R. Richards-Kortum, *Nanomedicine* **2006**, *1*, 23–30.
- [14] C. Witte, V. Martos, H. M. Rose, S. Reinke, S. Klippel, L. Schröder, C. P. Hackenberger, *Angew. Chem. Int. Ed.* **2015**, *54*, 2806–2810; *Angew. Chem.* **2015**, *127*, 2848–2852.
- [15] X. Song, R. D. Airan, D. R. Arifin, A. Bar-Shir, D. K. Kadayakara, G. Liu, A. A. Gilad, P. C. van Zijl, M. T. McMahon, J. W. Bulte, *Nat. Commun.* **2015**, *6*, 6719.
- [16] P. Caravan, J. J. Ellison, T. J. McMurry, R. B. Lauffer, *Chem. Rev.* **1999**, *99*, 2293–2352.
- [17] M. F. Bellin, *Eur. J. Radiol.* **2006**, *60*, 314–323.
- [18] a) R. Xie, S. Hong, L. Feng, J. Rong, X. Chen, *J. Am. Chem. Soc.* **2012**, *134*, 9914; b) R. Xie, L. Dong, R. Huang, S. Hong, R. Lei, X. Chen, *Angew. Chem. Int. Ed.* **2014**, *53*, 14082; *Angew. Chem.* **2014**, *126*, 14306.
- [19] P. V. Chang, J. A. Prescher, E. M. Sletten, J. M. Baskin, I. A. Miller, N. J. Agard, A. Lo, C. R. Bertozzi, *Proc. Natl. Acad. Sci. USA* **2010**, *107*, 1821–1826.
- [20] Y. Kita, Y. Miura, J. Furukawa, M. Nakano, Y. Shinohara, M. Ohno, A. Takimoto, S. Nishimura, *Mol. Cell. Proteomics* **2007**, *6*, 1437–1445.
- [21] N. Kaliss, D. Pressman, *Proc. Soc. Exp. Biol. Med.* **1950**, *75*, 16–20.
- [22] R. Weissleder, H. C. Cheng, E. Marecos, K. Kwong, A. J. Bogdanov, *Eur. J. Cancer* **1998**, *34*, 1448–1454.
- [23] H. Maeda, J. Wu, T. Sawa, Y. Matsumura, K. Hori, *J. Controlled Release* **2000**, *65*, 271–284.
- [24] S. Aime, C. Cabella, S. Colombatto, S. G. Crich, E. Gianolio, F. Maggioni, *J. Magn. Reson. Imaging* **2002**, *16*, 394–406.

Received: October 21, 2015

Published online: December 3, 2015